Physical Separation in Science and Engineering,
September–December 2004, Vol. 13, No. 3–4, pp. 89–99

Taylor & Francis
Taylor & Francis Group

MODELLING STUDIES ON A 100 mm WATER-INJECTION CYCLONE

K. UDAYA BHASKAR[a,*], B. GOVINDARAJAN[a], J.P. BARNWAL[a], K.K. RAO[b] and T.C. RAO[c]

[a]*Regional Research Laboratory, Bhopal – 462 026, India;* [b]*Department of Geology, Barkatullah University, Bhopal – 462 026, India;* [c]*Advisor, Environment Planning & Co-ordination Organisation (EPCO), Bhopal – 462 026, India*

(Received 18 May 2004; In final form 6 July 2004)

Test work on a 100 mm water-injection cyclone was carried out using a ground lead-zinc ore. Experiments were conducted varying the vortex finder diameter, spigot diameter, feed inlet pressure and injection water rate. The effect of variables on the performance of the water-injection cyclone in terms of slurry throughput and corrected cut-size are presented. A set of equations have been developed for predicting the performance of a water-injection cyclone. Further, the reduced efficiency curve was quantified to predict the size distribution of water-injection cyclone products.

Keywords: Water-injection cyclone; Corrected cyclone cut-size; Minimum distribution point; Reduced efficiency curve

1. INTRODUCTION

Water-injection cyclone (Fig. 1(a)) can be visualized as a normal hydrocyclone with an injection water assembly above the apex. Inside the injection water assembly (Fig. 1(b)) water is jacketed between two cylindrical portions. The outer cylinder of the bigger radius is a solid body and the inner cylindrical portion with a smaller radius is provided with tangential inlet holes at the middle of its height on the periphery. Water, which is injected tangentially, travels transversely towards the cyclone axis through the underflow slurry. In this process, the feed water reporting into the underflow will be displaced by injected water. This in turn carries out the entrapped fines into the overflow. Above the injection water assembly and below the conical portion of the cyclone, a truncated cone arrangement is provided to restrict the direct contact of the underflow slurry with

*Corresponding author. E-mail: kubhaskar2001@yahoo.com

ISSN 1478-6478 print: ISSN 1478-6486 online
DOI: 10.1080/14786470412331286580

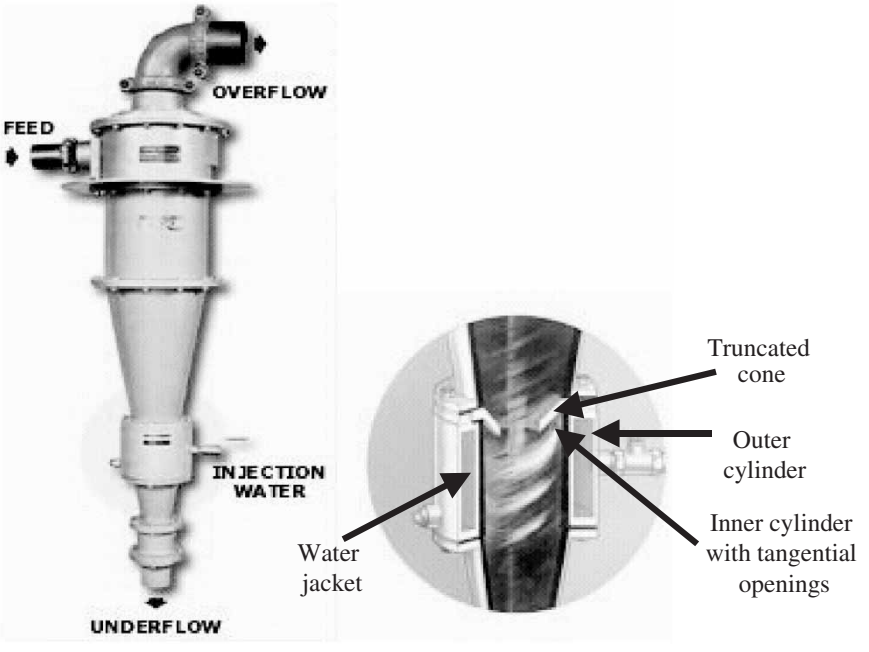

FIGURE 1 Water-injection cyclone (A) and injection water assembly (courtesy Krebs Engineers) (B).

the water injection holes. This arrangement also avoids the direct entry of injected water into the cyclone body.

The applications of a water-injection cyclone in order to obtain an underflow product relatively free of fines was available in the literature [1–7]). These studies have indicated the potential application in the coal and other industrial mineral sectors where the specific gravity differential between valuable minerals and gangue is small.

However, in the case of lead-zinc base metal ores, during grinding galena and sphalerite (the major lead-zinc bearing minerals in the ore) being brittle tend to be segregated at finer sizes than the gangue. Considerable portions of lead and zinc mineral particles below the cut-size of the cyclone, report to underflow along with feed water. Attempts made to recover these liberated heavy mineral particles into the overflow product using a water-injection cyclone have indicated that considerable amounts of liberated mineral fines (below 25 μm) can be recovered into the overflow product [8], which otherwise would report in major amounts in the underflow product of a normal hydrocyclone.

In the present study, the established models of Lynch and Rao [9] were adopted to model the results obtained by treating a typical ground lead-zinc ore in a standard Krebs KH 4 Cyclowash model (water-injection cyclone, supplied from Krebs Engineers). In order to obtain the corrected cyclone cut size for a particular experiment, the actual partition numbers were corrected by a factor, which is the minimum partition value for that experiment.

Further, the established Plitt's equation [10] was used to define the reduced efficiency curve. The details of the experimental programme and the methodology adopted are discussed in the following sections.

2. EXPERIMENTAL

2.1. Sample Collection and Characterization

The lead-zinc ground ore sample was collected from the operating plant at Rampura-Agucha Mines of Hindustan Zinc Limited, India. The sample slurry was filtered, dried and collected adopting standard sampling techniques [11]. A representative ore sample was examined for mineral phase identification using a X-ray diffraction (XRD) technique, size analysis and size-by-size metal and mineral distribution. The XRD studies have indicated the presence of galena and sphalerite as the abundant ore minerals of lead and zinc.

The size-by-size percentage weight report of the sample is presented in Fig. 2. The figure indicates that 90.4% of the material passed through 212 μm and 31.0% of the material is in the form of fines below 25 μm. The figure also indicates the cumulative lead and zinc metal distribution. A minimum lead and zinc content of 1.76% and 4.88% respectively can be observed at a coarsest fraction below 300 μm. Similarly the lead and zinc contents of 3.0% and 5.9% respectively can be observed in the aggregate feed. It may be observed from the figure that lead and zinc content increase with decreases in particle size.

Different size fractions obtained from the sieve analysis were examined under a microscope for mineralogical distribution. The size-by-size mineralogical composition of the ground lead-zinc ore sample is presented in Fig. 3. It may be noted from the figure that the amount of heavy minerals (galena, sphalerite, pyrite and chalcopyrite) increases with decreases in particle size. Conversely, the amount of lighter gangue minerals decreases with a reduction of particle size. For example, the coarsest fraction,

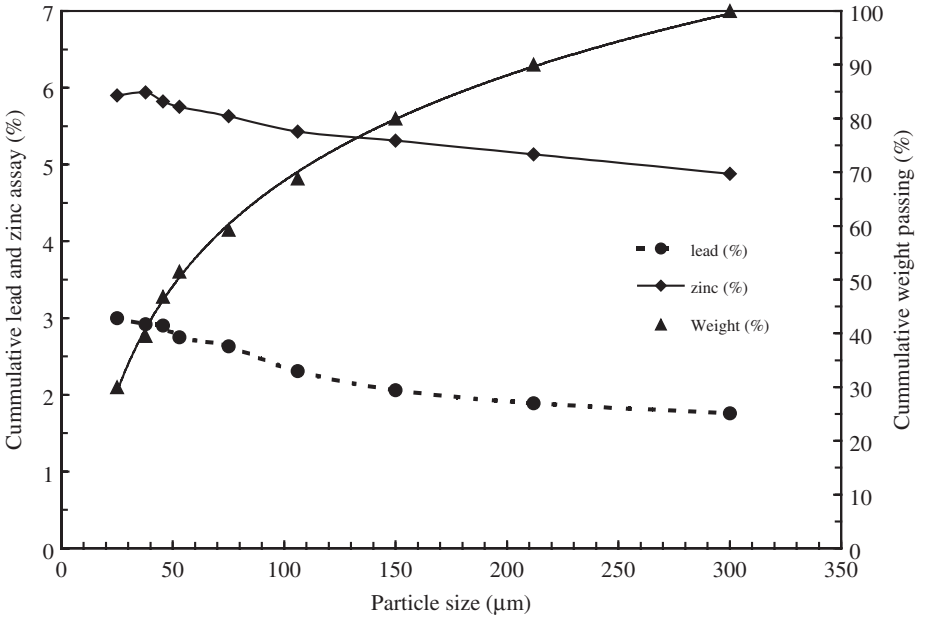

FIGURE 2 Size analysis and size by size lead and zinc metal distribution.

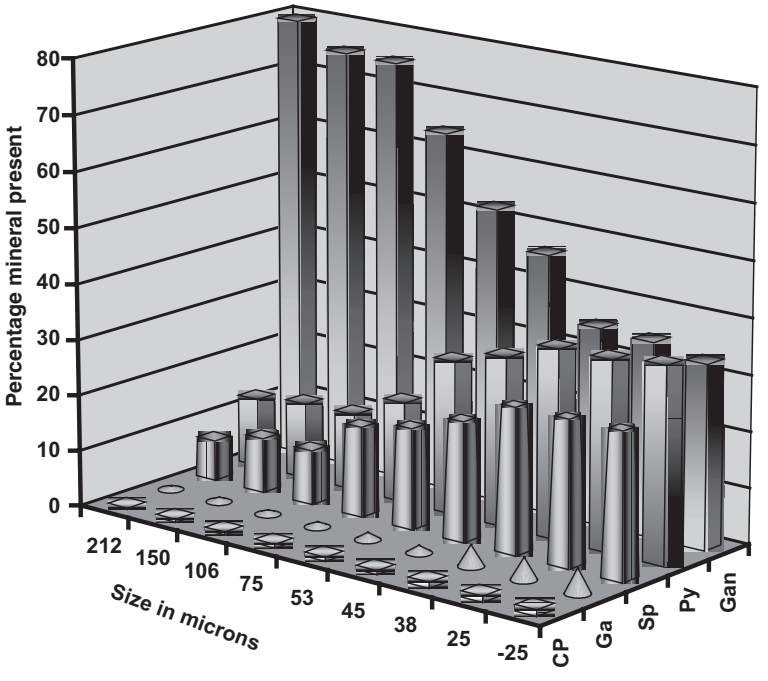

FIGURE 3 Size by size mineral distribution; CP: Chalcopyrite; Ga: Galena; Sp: Sphalerite; Py: Pyrite; Gan: Gangue.

e.g. $-300+212\,\mu m$ size contained only 20.4% of heavy minerals and the finest fraction, $-25\,\mu m$ size contained as high as 67.4% of heavy minerals. This indicates preferential grinding of metallic minerals over the gangue. It may further be noted from the figure that the abundance of minerals present in the sample (except at fines below $25\,\mu m$) is in the following order:

Gangue > Pyrite > Sphalerite > Galena > Chalcopyrite

The lead, zinc, iron and copper minerals (galena, sphalerite, pyrite and chalcopyrite) with specific gravities between 7.5 and 4.0, are heavier than the associated gangue minerals with typical specific gravity values around 2.6.

2.2. Experimental Set-up and Test Procedure

The test-rig used in the experimental work (Fig. 4) consisted of a feed slurry tank (200l) and an injection water tank (100l) mounted on a stable platform. The bottom of the feed slurry tank was connected to a centrifugal pump driven by a three-phase, 5.5 kW motor. The outlet of the pump was connected to the feed inlet of a 100 mm water-injection cyclone positioned vertically above the feed slurry tank. A by-pass pipe with a control valve was connected to the pump outlet line to obtain the required pressure drop inside the cyclone.

A pre-selected vortex finder, truncated cone and spigot were fitted to the body of the water-injection cyclone. A measured amount of solids and water were mixed in the feed tank to achieve solids consistency of 10% (by weight) in the feed pulp. Initially, the injection water was pumped into the cyclone at a pre-selected rate and then the feed

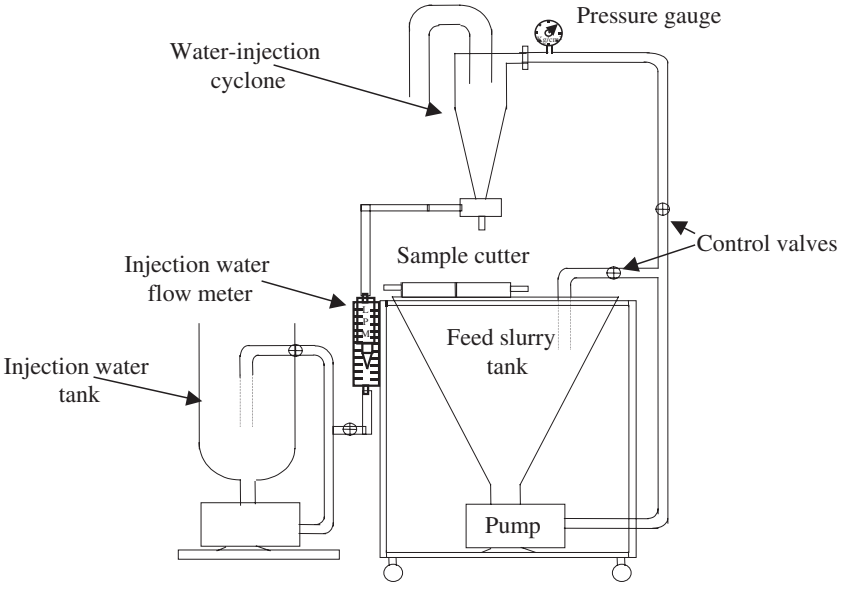

FIGURE 4 Water-injection cyclone test-rig.

slurry was pumped at the required pressure. Timed samples from both the overflow and underflow slurry streams were collected simultaneously. The slurry and solid weights of the products were measured and solid samples were used for size analysis.

2.3. Experimental Design

A set of 24 experiments were carried out. Experiments were differentiated by varying important variables such as the vortex finder diameter; the combination of truncated cone diameter and spigot diameter (at each diameter of the spigot opening, a truncated cone of appropriate size was inserted), the feed inlet pressure and injection water rate were studied.

3. RESULTS AND DISCUSSION

The test conditions and the results obtained are presented in Table I. The effects of variables and models developed are discussed in the following sections.

3.1. Effect on Slurry Throughput

The slurry throughput is a combined value of feed slurry rate and injected water rate. It may be observed from the table that an increase in vortex finder diameter, spigot diameter, feed pressure and injection water rate, in general increases the slurry throughput. An increase in the slurry throughput for an increase in vortex finder diameter and spigot diameter could be due to increased openings for passage. Increased slurry throughput at higher feed pressure could be due to increased centrifugal field, which reduces the residence time of slurry in the cyclone system.

TABLE I Experimental conditions and test results obtained from a 100 mm water-injection cyclone

Ex. No.	*VF*	*SPIG*[b]	*Pressure*	*IR*	*Q*	*MDP*	d_{50c}
1	25.40	26.97	0.56	1.20	10.5	47.0	17.5
2	25.40	26.97	1.12	1.20	13.7	37.7	14.2
3	31.75	26.97	0.56	1.20	11.3	24.5	20.2
4	31.75	26.97	1.12	1.20	15.3	27.4	16.3
5	31.75	22.23	0.56	1.20	10.7	9.3	41.4
6	31.75	22.23	1.12	1.20	14.7	10.0	26.8
7	25.40	22.23	0.56	1.20	9.7	16.0	35.6
8	25.40	22.23	1.12	1.20	12.6	20.1	20.0
9	25.40	22.23	0.56	2.40	10.0	22.8	22.5
10	25.40	22.23	1.12	2.40	13.5	28.2	16.6
11	31.75	22.23	0.56	2.40	11.5	11.2	28.0
12	31.75	22.23	1.12	2.40	15.6	18.9	17.5
13	31.75	26.97	0.56	2.40	12.3	20.7	20.0
14	31.75	26.97	1.12	2.40	17.0	22.1	16.6
15	25.40	26.97	0.56	2.40	10.8	33.2	19.3
16	25.40	26.97	1.12	2.40	14.8	37.5	14.5
17	25.40	26.97	0.56	3.60	12.4	14.3	26.2
18	25.40	26.97	1.12	3.60	16.4	31.4	14.9
19	31.75	26.97	0.56	3.60	13.8	3.0	56.2
20	31.75	26.97	1.12	3.60	18.8	19.8	16.9
21[a]	31.75	22.23	0.56	3.60		No solids were reported	
22	31.75	22.23	1.12	3.60	17.7	12.3	26.2
23[a]	25.40	22.23	0.56	3.60		No solids were reported	
24	25.40	22.23	1.12	3.60	15.6	11.3	19.3

Note. [a]Experiments 21 and 23 were not considered in developing equations.
[b]Truncated cone diameters of 19.05 and 25.4 mm are used for spigot diameters 22.23 and 26.97 mm respectively (standard truncated cones supplied by Krebs Engineers).
VF: vortex finder diameter (mm).
SPIG: spigot diameter (mm).
IR: injection water rate (metric tonnes per hour).
Q: slurry throughput including injection water (metric tonnes per hour).
MDP: minimum distribution points (%).
d_{50c}: corrected cut-size in microns.

The equation relating the variables and the slurry throughput is as follows:

$$Q = 0.584\,\mathrm{VF}^{0.570}\,\mathrm{SPIG}^{0.369}\,P^{0.44}\,\mathrm{IR}^{0.168} \quad (1)$$
$$(R^2 = 0.980\text{: standard error} = 0.417)$$

3.2. Prediction of Corrected Cyclone Cut-size d_{50c}

The actual partition curve relating the percentage distribution of each size fraction into the underflow product and the particle size is corrected by applying a correction factor R_f, which is equal to the mass fraction of the feed water reporting to the underflow. However, the R_f value could not be estimated in a water-injection cyclone due to the additional water source. Thus, the minimum distribution point (MDP) on the actual partition curve (Fig. 5) for an individual experiment was used as a correction factor. From the corrected efficiency curve the cyclone cut-sizes d_{50c} were generated.

It may also be observed from Table I that there is a general trend to increase the corrected cut size with an increase in the vortex finder diameter and injection water

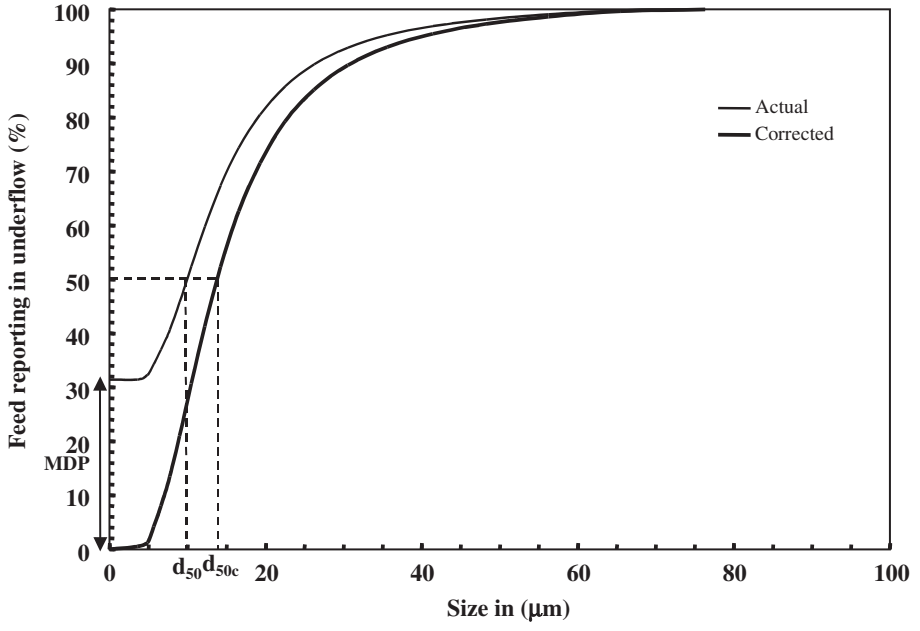

FIGURE 5 Typical uncorrected and corrected classification curves.

rate and a decrease in spigot diameter and feed pressure. An increase in the vortex finder diameter increases slurry flow opening into the overflow. Similarly, an increase in injection water rate increases the vertical push on the particles, which not only results in fine displacement from the underflow, but also pushes some portion of coarse material report into the overflow resulting in increased cyclone cut size.

An increase in the spigot diameter widens the passage for materials in the downward direction, which results in increased fines entrapment in the underflow due to insufficient residence time. The lower values of cut size achieved at higher feed pressures may be explained by an increased centrifugal force on particles at higher pressures that results in finer fractions also reporting to higher radial distances in the cyclone body and reporting through the underflow.

The relationship between the d_{50c} values and the variables is presented in Eq. (2):

$$\log_{10} d_{50c} = 0.032\,VF - 0.11\,\mathrm{SPIG} - 0.89P + 0.034\,\mathrm{IR} + 5.503 \quad (2)$$
$$(R^2 = 0.90\text{: standard error} = 2.810)$$

3.4. Prediction of Minimum Distribution Point (MDP) Values

Having corrected the actual distribution curves with the MDP values, it is necessary to develop a relationship for predicting the MDP values for a complete model. The equation relating the variables and the MDP values is as follows:

$$\log_{10} \mathrm{MDP} = -0.07\,\mathrm{VF} + 0.153\,\mathrm{SPIG} + 0.066\,P - 0.087\,\mathrm{IR} + 1.352 \quad (3)$$
$$(R^2 = 0.932\text{: standard error} = 2.82)$$

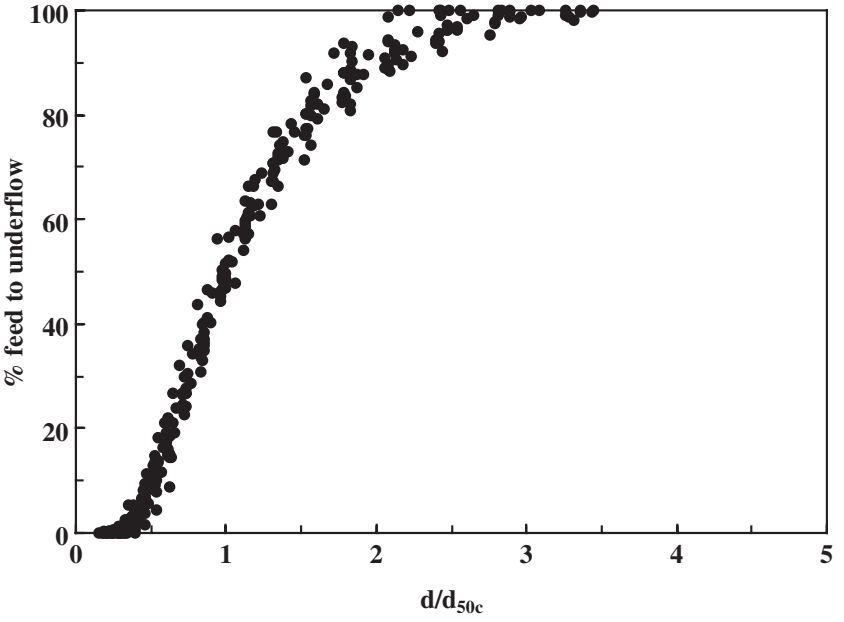

FIGURE 6 Reduced efficiency curve obtained for the data on 100 mm water-injection cyclone.

The equation indicates that the MDP values in the water-injection cyclone decreases with an increasing vortex finder diameter and injection water rate. The equation also indicates that the MDP values increase with an increasing spigot diameter and feed pressure. These observations may be attributed to the fact that the amount of fines in the underflow product decreases at increased levels of vortex finder diameter and injection water, and at decreased levels of spigot opening and feed pressure.

3.5. Prediction of the Reduced Efficiency Curve

The corrected distribution points (Y) obtained at different test conditions are plotted against reduced sizes, i.e. d/d_{50c} [11] in Fig. 6. It can be observed from the figure that the reduced efficiency curve remains unchanged over a wide range of design and operating conditions of water-injection cyclone. The equation relating the reduced size and the corrected distribution data is as follows:

$$Y = 100\left[1 - e^{0.6931\{d/d_{50c}\}^{2.239}}\right] \tag{4}$$

$$(R^2 = 0.981\text{: standard error} = 4.831)$$

The actual and predicted values of the slurry throughput, d_{50c}, MDP values and distribution points are presented in Figs 7–10, respectively. It may be observed from the figures that the actual and predicted values are close to diagonal lines connecting the minimum and maximum values in each figure, which indicates good prediction levels of these equations.

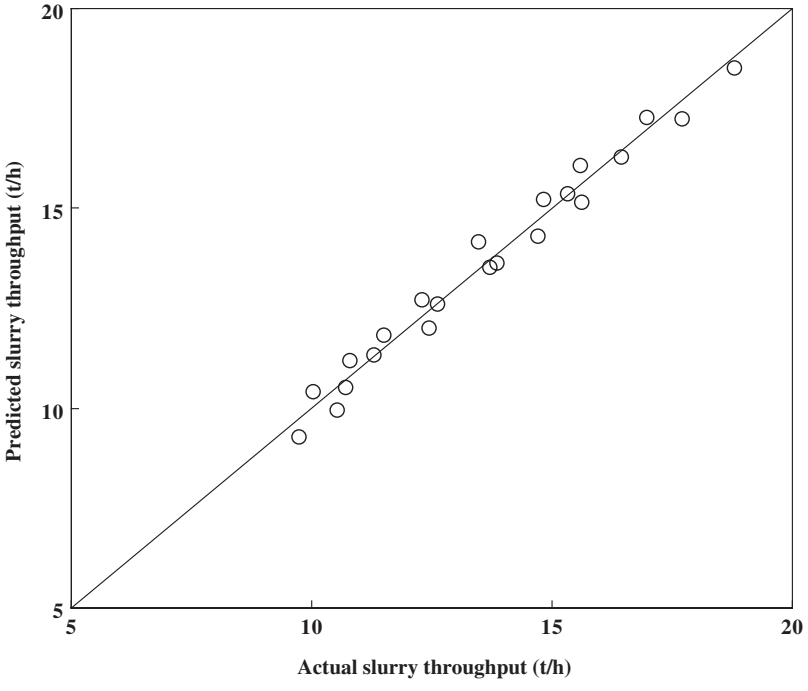

FIGURE 7 Relationship between actual and predicted values of slurry throughput.

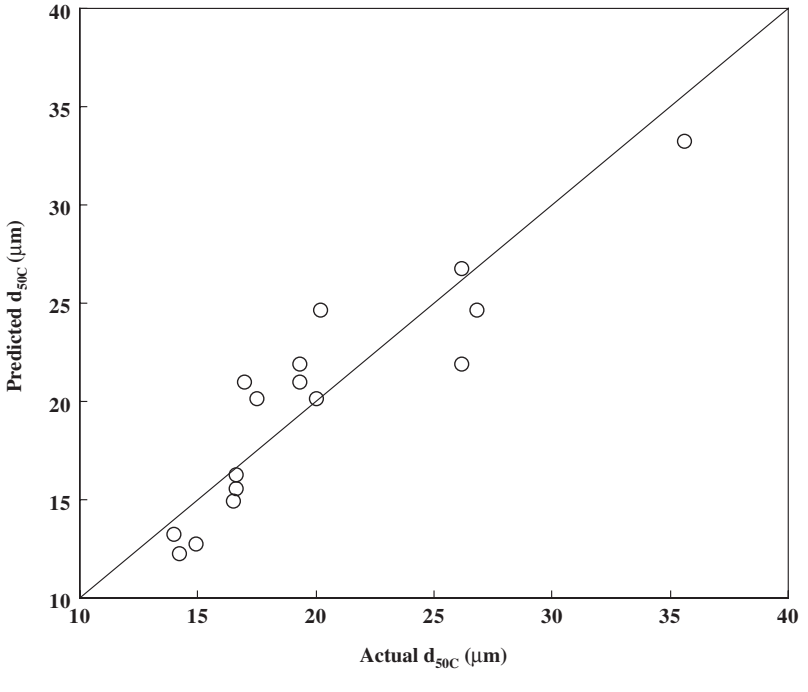

FIGURE 8 Relationship between actual and predicted values of corrected cut-size, d_{50c}.

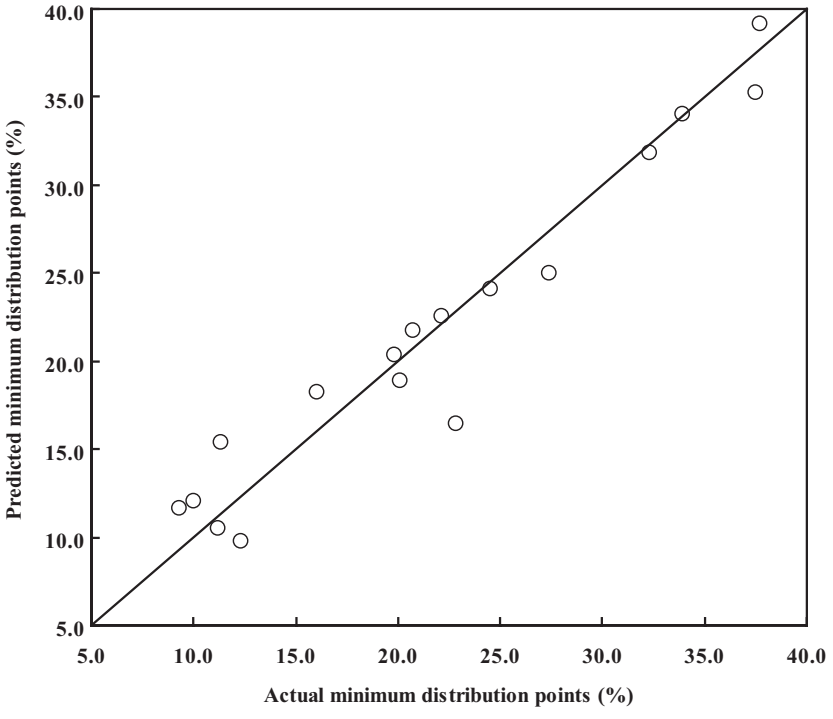

FIGURE 9 Relationship between actual and predicted values of minimum distribution points.

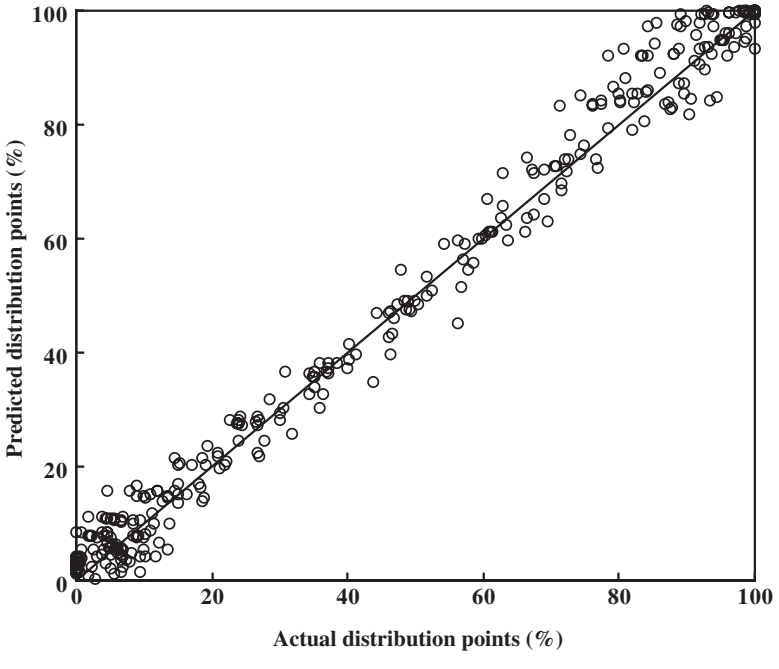

FIGURE 10 Relationship between actual and predicted values of distribution points.

4. CONCLUSION

The methodology used for predicting hydrocyclone performance can also be applied for predicting the performance of a water-injection cyclone by applying MDP values to obtain the corrected cyclone cut-sizes. The following four equations together predict the classification performance of a 100 mm water-injection cyclone:

$$Q = 0.584\,\mathrm{VF}^{0.570}\,\mathrm{SPIG}^{0.369}\,P^{0.442}\,\mathrm{IR}^{0.168}$$

$$\log_{10} \mathrm{d}_{50\mathrm{c}} = 0.032\,\mathrm{VF} - 0.11\,\mathrm{SPIG} - 0.89P + 0.034\,\mathrm{IR} + 5.503$$

$$\log_{10} \mathrm{MDP} = -0.07\,\mathrm{VF} + 0.153\,\mathrm{SPIG} + 0.066\,P - 0.087\,\mathrm{IR} + 1.352$$

$$Y = 100\left[1 - \mathrm{e}^{0.6931\{\mathrm{d}/\mathrm{d}_{50\mathrm{c}}\}^{2.239}}\right]$$

References

[1] D.A. Dahlstrom, Fundamentals and applications of the liquid cyclone. *Chem. Eng. Prog. Symp. Series, American Institure of Chemical Engineers*, **50**(15) (1954), 41.
[2] D.F. Kelsall, A further study of the hydraulic cyclone. *J. Chem., Metall. Min. Soc. South Africa*, September (1955), 125–152.
[3] D.F. Kelsall and J.A. Homes, Improvement in classification efficiency in hydraulic cyclones by water injection. In: *Proc. 5th Min. Proc. Congress 1960*, Paper 9, Inst. of Mining and Metallurgy, pp. 159–170.
[4] D. Bradley, *The Hydrocyclone*, Pergamon Press, London, 1965.
[5] B. Firth, D. Edwards, C. Clarkson and M. O'Brien, The impact of classification on coal preparation performance. In: *Proc. 7th Austral. Coal Prep. Conf.*, Paper E2, Australian Coal Preparation Society, 1995, pp. 250–276.
[6] D.D. Patil and T.C. Rao, Classification evaluation of water injected hydrocyclone. *Min. Engn.*, **12**(12) (1999), 1527–1532.
[7] R.Q. Honaker, A.V. Ozsever, N. Singh and B.K. Parekh, Apex water injection for improved hydrocyclone classification efficiency. *Min. Eng.* **14**(11) (2001), 1445–1458.
[8] K. Udaya Bhaskar, B. Govindarajan, J.P. Barnwal, K.K. Rao and T.C. Rao, Comparative performance study on a 100 mm water-injection cyclone and a hydrocyclone. In: *Proc. Int. Seminar Min. Process. Technol.*, Hyderabad, 2001, pp. 63–67.
[9] A.J. Lynch and T.C. Rao, Modelling and scale-up of hydrocyclone classifiers. In: *Proc. 11th Int. Min. Process. Congr.*, Cagliari, 1975, pp. 9–25.
[10] L.R. Plitt, A mathematical model of the hydrocyclone classifier. *CIM Bull.* (1976), 114–122.
[11] B.A. Wills, *Mineral Processing Technology*, Pergamon Press, Oxford, 1997, pp. 232–234.